Endothelial cell-specific redox gene modulation inhibits angiogenesis but promotes B16F0 tumor growth in mice

Yura, Yoshimitsu; Chong, Brian S.H.; Johnson, Ryan D.; Watanabe, Yosuke; Tsukahara, Yuko; Ferran, Beatriz

Published in:
FASEB journal : official publication of the Federation of American Societies for Experimental Biology

DOI:
10.1096/fj.201900786R

Publication date:
2019

Document Version
Peer reviewed version

The FASEB Journal
The Journal of the Federation of American Societies for Experimental Biology
All Articles | Submit | Subscribe | What's New | RSS

FASEB J. 2019 Dec; 33(12): 14147–14158.
Published online 2019 Oct 26.
doi: 10.1096/fj.201900786R: 10.1096/fj.201900786R

PMCID: PMC6894059
PMID: 31647879

Endothelial cell-specific redox gene modulation inhibits angiogenesis but promotes B16F0 tumor growth in mice

Yoshimitsu Yura,[*,1,2] Brian S. H. Chong,[*,1] Ryan D. Johnson,[*] Yosuke Watanabe,[*,3] Yuko Tsukahara,[*] Beatriz Ferran,[*] Colin E. Murdoch,[*,4] Jessica B. Behring,[*] Mark E. McComb,[†] Catherine E. Costello,[†] Yvonne M. W. Janssen-Heininger,[‡] Richard A. Cohen,[*] Markus M. Bachschmid,[*] and Reiko Matsui[*,5]

[*]Department of Medicine, Vascular Biology Section, Whitaker Cardiovascular Institute, Boston University School of Medicine, Boston, Massachusetts, USA;
[†]Cardiovascular Proteomics Center, Boston University School of Medicine, Boston, Massachusetts, USA;
[‡]Department of Pathology and Laboratory Medicine, University of Vermont, Burlington, Vermont, USA
[1]These authors contributed equally to this work.
[2]Current affiliation: University of Virginia School of Medicine, Charlottesville, VA, USA.
[3]Current affiliation: Department of Internal Medicine II, University of Yamanashi, Yamanashi, Japan.
[4]Current affiliation: Systems Medicine, University of Dundee, Dundee, United Kingdom.
[5]Correspondence: Vascular Biology Section, Boston University School of Medicine, 650 Albany St. X-729, Boston, MA 02118, USA., E-mail: rmatsui@bu.edu

Received 2019 Mar 26; Accepted 2019 Sep 17.

Abstract

Glutaredoxin-1 (Glrx) is a small cytosolic enzyme that removes *S*-glutathionylation, glutathione adducts of protein cysteine residues, thus modulating redox signaling and gene transcription. Although Glrx up-regulation prevented endothelial cell (EC) migration and global Glrx transgenic mice had impaired ischemic vascularization, the effects of cell-specific Glrx overexpression remained unknown. Here, we examined the role of EC-specific Glrx up-regulation in distinct models of angiogenesis; namely, hind limb ischemia and tumor angiogenesis. EC-specific Glrx transgenic (EC-Glrx TG) overexpression in mice significantly impaired EC migration in Matrigel implants and hind limb revascularization after femoral artery ligation. Additionally, ECs migrated less into subcutaneously implanted B16F0 melanoma tumors as assessed by decreased staining of EC markers. Despite reduced angiogenesis, EC-Glrx TG mice unexpectedly developed larger tumors compared with control mice. EC-Glrx TG mice showed higher levels of VEGF-A in the tumors, indicating hypoxia, which may stimulate tumor cells to form vascular channels without EC, referred to as vasculogenic mimicry. These data suggest that impaired ischemic vascularization does not necessarily associate with suppression of tumor growth, and that antiangiogenic therapies may be ineffective for melanoma tumors because of their ability to implement vasculogenic mimicry during hypoxia.—Yura, Y., Chong, B. S. H., Johnson, R. D., Watanabe, Y., Tsukahara, Y., Ferran, B., Murdoch, C. E., Behring, J. B., McComb, M. E., Costello, C. E., Janssen-Heininger, Y. M. W., Cohen, R. A., Bachschmid, M. M., Matsui, R. Endothelial cell-specific redox gene modulation inhibits angiogenesis but promotes B16F0 tumor growth in mice.

Keywords: *S*-glutathionylation, glutaredoxin, vasculogenic mimicry, vascular, melanoma

Oxidants, or reactive oxygen and nitrogen species, have been recognized to play an essential role in signal transduction (1–3). Oxidants promote protein *S*-glutathionylation, which is a reversible post-translational modification of protein cysteine residues with the tripeptide glutathione (GSH). Protein *S*-glutathionylation can regulate a variety of cellular processes, including transcription, apoptosis, and cytoskeletal assembly (4, 5). De-glutathionylation (removal of GSH adducts) can occur spontaneously but is more efficiently driven by the catalyzing enzyme glutaredoxin-1 (Glrx) (4). Therefore, Glrx is a crucial molecule for redox signaling regulated by the protein *S*-glutathionylation.

Angiogenesis is the process of forming new blood vessels from preexisting ones. Endothelial cell (EC) migration is an essential component of angiogenesis, which is required for many physiologic and pathologic processes, including wound healing, tissue regeneration, and tumor growth (6). Protein *S*-glutathionylation can regulate angiogenesis through several target proteins. The formation of a GSH adduct on the cysteine-674 of sarco/endoplasmic reticulum calcium ATPase activates the Ca^{2+} pump and promotes EC migration (7, 8). As a consequence, overexpression of Glrx inhibits *in vitro* EC migration and *in vivo* ischemic limb revascularization in global Glrx transgenic mice (9). Increased *S*-glutathionylation also inhibits Ras-related C3 botulinum toxin substrate (Rac)1, a small Rho GTPase, and promotes EC permeability (10), an initial step for EC migration. We further demonstrated that *S*-glutathionylation of cysteine in the oxygen-dependent degradation domain of hypoxia-inducible factor (HIF)-1α stabilizes HIF-1α and increases angiogenic factors (11). Consistent with these findings, increased protein *S*-glutathionylation by Glrx deletion promotes mouse ischemic limb revascularization after femoral artery ligation (11). Thus, up-regulated Glrx inhibits angiogenic pathways (12).

Because previous studies used global transgenic or knockout mice, we explored the tissue-specific role of Glrx and its regulation of protein *S*-glutathionylation. Tissue components, including EC, skeletal muscles, and myeloid cells, regulate the angiogenic process (9, 13). In this study, we examined the role of up-regulated Glrx in ECs on ischemic limb vascularization and tumor angiogenesis. Comparable to our earlier *in vitro* EC study, EC-specific Glrx transgenic (EC-Glrx TG) overexpressing mice showed impaired EC migration, resulting in severely diminished blood flow recovery in ischemic limbs. Unexpectedly, subcutaneous melanoma tumor growth was promoted in EC-Glrx TG mice, despite repressed EC-dependent angiogenesis, suggesting that the tumor has a secondary mechanism to acquire its blood supply.

Furthermore, we analyzed EC protein *S*-glutathionylation regulated by Glrx using a quantitative cysteine labeling strategy followed by mass spectrometric analysis, using methods we reported earlier (14). Biologic pathway analysis indicated that EC-Glrx regulates the function of an array of proteins, including metabolic signaling molecules that may be important in the tumor microenvironment.

MATERIALS AND METHODS

Cell culture and reagents

B16F0 mouse melanoma cells were a gift from Dr. Nader Rahimi (Boston University School of Medicine) and maintained in DMEM with 4.5 g/L D-glucose and 10% fetal bovine serum. Human cardiac microvascular ECs (HCMVECs) were obtained from American Type Culture Collection (ATCC; Manassas, VA, USA) and maintained in EGM-2 MV medium (Lonza Group, Basel, Switzerland) with 5% fetal bovine serum. Anti-Glrx antibody (AGRX-03; IMCO, Stockholm, Sweden) was provided by Cayman Chemicals (Ann Abor, MI, USA). Anti-CD31 antibodies (ab28364, RRID:AB_726362) were from Abcam (Cambridge, MA, USA) for immunofluorescence and Servicebio (GB11063-3; Woburn, MA, USA) for immunohistochemistry. Anti-FLAG antibody (F7425) was from MilliporeSigma (Burlington, MA, USA). Fluorescein-labeled *Griffonia simplicifolia* lectin I isolectin B4 (FL-1201) was from Vector Laboratories (Burlingame, CA, USA). Recombinant human VEGF was purchased from R&D Systems (Minneapolis, MN, USA). All reagents were purchased from Thermo Fisher Scientific (Waltham, MA, USA) unless specified otherwise.

EC-specific Glrx overexpressing mice

C57BL/6 VEcad-tTA mice (The Jackson Laboratory, Bar Harbor, ME, USA) and tet-*O*-Glrx mice (15) were bred to create EC-Glrx TG mice. The double transgenic (EC-Glrx TG) mice express tetracycline transactivator (tTA) driven by vascular endothelial (VE)-cadherin (VEcad) promoter in EC, which binds to the tetracycline operating element, leading to FLAG-Glrx expression. Transgene tTA was confirmed by PCR of genomic DNA using primers 5′-CGCTGTGGGGCATTTTACTTTAG-3′and 5′-CATGTCCAGATCGAAATCGTC-3′, FLAG-Glrx expression was confirmed with primers 5′-AACAACACCAGTGCGATTCA-3′ and 5′-GGGCTTAGATGGCGATACTC-3′. Doxycycline (DOX) in drinking water binds to tTA and suppresses FLAG-Glrx transgene expression in EC-Glrx TG mice. Mice received DOX (1.5 mg/L) until 4 wk old to avoid developmental effects of EC-Glrx overexpression for ischemic limb studies. VEcad single transgenic and wild-type littermates were used as controls. All studies for tumor growth were performed without DOX administration. Boston University Institutional Animal Care and Use Committee approved the study protocol.

Hind limb ischemia model

All mice were treated with DOX *in utero* through 4 wk of age, and then they were taken off DOX for 8 wk. Male mice at 12 wk old were anesthetized with ketamine (100 mg/kg) and xylazine (10 mg/kg) through intraperitoneal injection. Hind limb ischemia was produced as previously described (11, 16). Briefly, after ligation of the left femoral artery proximal to the superficial epigastric artery branch and the tibial artery branch, the segment of the femoral artery between ligations was excised. Buprenorphine (0.5 mg/kg) was given before and after surgery for 3 d. Blood flow was analyzed using laser doppler (Moor Instruments, Wilmington, DE, USA) on plantar aspects of the feet before and after surgery for 14 d. Blood flow recovery was expressed as the ratio of ischemic (left) to nonischemic (right) foot. Necrosis progression up to the knee was considered a criterion for euthanasia. The Institutional Animal Care and Use Committee at Boston University approved the animal study protocols (AN15292).

EC migration *in vivo* assay

Matrigel (500 µl) was implanted subcutaneously in EC-Glrx TG and control mice for 2 wk with or without VEGF (100 ng/ml). Excised Matrigel plugs were homogenized to measure hemoglobin content by using a Hemoglobin Colorimetric Assay Kit (Cayman Chemicals) (17). For immunohistochemistry, excised Matrigel plugs were immersed in 4% paraformaldehyde for 4 h and then transferred to 20% sucrose for 18 h at room temperature followed by embedding in optimal cutting temperature (OCT) compound. A frozen section with 14 µm thickness was placed on a glass slide, returned to room temperature, and fixed again with 4% paraformaldehyde for 10 min and stained with anti-CD31 antibody (Servicebio).

Tumor angiogenesis model

Tumor angiogenesis was analyzed in adult mice (3–4-mo-old; males and females) using B16F0 murine melanoma cell implants. Adherent B16F0 cells were harvested, and single-cell suspensions of 4×10^5 cells in 200 µl of Matrigel were injected subcutaneously into the left dorsum. Mice were euthanized 2 wk after cell inoculation. Tumors were removed, weighed, sized, and processed for further histologic and biochemical analyses. Tumor volume was calculated using the ellipsoid volume formula, which is $V = \pi/6 \times \text{length} \times \text{width} \times \text{height}$ (18).

B16F0 tube formation assay

B16F0 melanoma cells cultured on matrix develop tube-like structures and form networks (19, 20). Briefly, 50 µl of Matrigel was plated in 96-well culture dishes and allowed to polymerize at 37°C for 1 h. B16F0 cells (2.5×10^4 cells/well) were plated on the Matrigel and incubated for 6 h under 1 or 20% O_2. Randomized fields were captured using an inverted microscope fitted with a digital camera (Spot Insight; Spot Imaging, Sterling Heights, MI, USA). The images were acquired using the Spot advanced software, and the network formation in each well was quantified by the number of intersections and total network length using ImageJ analysis software (National Institutes of Health, Bethesda, MD, USA). The intersections were measured by counting the number of connections between 2 or more capillary-like structures per field. The length of the networks was quantified by the sum of total branch length per field. To test the effect of VEGF-A, B16F0 1×10^4 cells/100 µl medium per well were used in a 96-well plate

with 50 µl of Matrigel coated for 1 h in 37°C. VEGF-A (5 or 10 ng/ml) was added in serum-free medium. Photos were taken under the microscope after 4 h. The Angiogenesis Analyzer macro tool for ImageJ was used to analyze phase contrast photos (Supplemental Fig. S3).

B16F0 proliferation assay

The cells were plated on 96-well plates ($0.2–0.4 \times 10^4$) in serum-free DMEM with or without VEGF. After 24 h, the medium was replaced with Hoechst 33342 solution (1 µg/ml; Thermo Fisher Scientific) for 10 min and washed with PBS followed by measuring nuclear staining with a microplate fluorescence reader (Infinite M1000 Pro; Tecan, Männedorf, Switzerland).

Quantitative PCR analysis

Total RNA was isolated from B16F0 tumors using the Quick-RNA MicroPrep Kit (R1050; Zymo Research, Irvine, CA, USA). We used tumors included from surface to center after resecting a part for histologic analysis. We confirmed that the ratio of absorbance at 260 and 280 nm was ~2.0, and the ratio of 260/230 nm was about 2.0. RT was performed to generate cDNA using the High-Capacity RNA to cDNA Kit (4387406; Thermo Fisher Scientific). Quantitative PCR was performed using gene-specific TaqMan primers: β-actin (ACTB; Mm00607939_s1), Fms-related tyrosine kinase 1 (Flt1; Mm01210863_m1), kinase insert domain receptor (Mm00440111_m1), platelet endothelial cell adhesion molecule (Pecam1; Mm01242584_m1), cadherin 5 (Mm00486938_m1), EPH receptor A2 (Mm00438726_m1), neuropilin 1 (Mm00435379_m1), and Glrx (Mm00728386_s1). Expression levels were analyzed by comparative C_t ($\Delta\Delta C_t$) to ACTB with CFX Maestro PCR software (Bio-Rad, Hercules, CA, USA).

Immunohistochemistry

Excised tumors were fixed overnight in 4% paraformaldehyde at 4°C. Samples were then cryoprotected in 10% sucrose overnight. Samples were frozen in OCT compound and cut into 10-µm sections. Slides were washed in PBS. Sections were blocked in 5% bovine serum albumin for 1 h, and antibodies were added into the blocking buffer. Sections were washed in PBS and incubated with the appropriate Alexa Fluor 488– or 594-conjugated secondary antibodies (1:200) and Hoechst 33342 solution for 1 h. Immunofluorescent CD31-stained areas were quantified using ImageJ, as previously described (21), by taking pictures from 5 random fields per tumor, imaging 6 tumors for each group. Similarly, fluorescence-conjugated isolectin B4 was used as an EC marker (22). For immunohistochemistry, the sections were treated with high-temperature citric acid buffer and then with 10% H_2O_2 for 15 min. After blocking with bovine serum albumin, the sections were incubated with anti-CD31 antibody (1:500, GB11326; Servicebio) in PBS overnight at 4°C. After the sections were washed, the horseradish peroxidase–conjugated goat anti-rabbit secondary antibody (1:200) in PBS was applied for 50 min. The slides were stained with AEC substrate (ab64252; Abcam) followed by hematoxylin staining.

Dextran perfusion

Dextran perfusion was carried out according to previously published methods (19). B16F0 tumor cells were subcutaneously injected as previously described. After 2 wk, mice were retro-orbitally injected with 100 µl Texas Red-labeled Dextran, 70K MW (Thermo Fisher Scientific) and euthanized 5 min postinjection. Tumors were prepared for immunohistochemistry with anti-CD31 and were imaged with a Keyence fluorescence microscope (BZ-9000; Keyence, Osaka, Japan).

Western blotting

Cells and tissue were lysed with 25 mM Tris·HCl, 150 mM NaCl, 10 mM EDTA, 1% Triton X-100, and 1× protease and phosphatase inhibitor mixture (PI78441). Samples were incubated with sample loading buffer (NP0007) for 5 min at 95°C. The protein concentration was measured with the DC assay (Bio-Rad). SDS-PAGE separated samples containing equal amounts of protein, and the proteins were transferred to PVDF membranes. After blocking with 5% skim milk in PBS with Tween 20 (0.1%) for 1 h, the

membranes were incubated with the specific antibodies overnight at 4°C, followed by horseradish peroxidase–conjugated secondary antibody for 1 h at room temperature. Images were visualized using ECL.

VEGF ELISA

VEGF protein levels in tumors were assessed by ELISA using a RayBio Mouse VEGF ELISA Kit (RayBiotech, Peachtreee Corners, GA, USA) according to the manufacturer's instructions. Data were normalized for total protein concentration.

Multiplex assay

Tumor lysate was analyzed in duplicate to determine the levels of cytokines and inflammatory markers, using a multiplex magnetic bead immunoassay (R&D Systems). Quantitation of this assay was performed by the Analytical Instrumentation Core at the Boston University School of Medicine on a Luminex Magpix instrument (Luminex, Austin, TX, USA) equipped with xPONENT 4.2 software. Milliplex Analyst Software v.5.1 (VigeneTech, Carlisle, MA, USA) was used to determine the concentration of each analyte.

Tandem mass tag labeling and liquid chromatography-tandem mass spectrometry

HCMVECs from ATCC were infected by an adenovirus expressing human Glrx or LacZ as control (9), and a set of cells was exposed to hypoxia (0.1% O_2) for 24 h followed by reoxygenation for 2 min. Cellular proteins from 4 groups were analyzed to detect reversibly modified protein thiols. Briefly, after free thiols were blocked with iodoacetamide, proteins were reduced with 1 mM tris-(2-carboxyethyl)-phosphine, and each sample was labeled with a different stable isotope-coded cysteine-reactive tandem mass tag (4-plex), digested with Trypsin/Lys C mix (Promega, Madison, WI, USA), and processed for liquid chromatography-tandem mass spectrometry (LC-MS/MS). The LC-MS/MS analyses were performed with a nanoAcquity UPLC nano-capillary high-performance LC system (Waters, Milford, MA, USA) coupled to a Q Exactive hybrid quadrupole-Orbitrap mass spectrometer (Thermo Fisher Scientific) equipped with a TriVersa NanoMate ion source (Advion, Ithaca, NY, USA). Spectra were acquired in the profile mode, and the data were searched using Peptide Shaker 1.16.15 (Compomics; *http://compomics.github.io/*). Tandem mass tags labeling was analyzed using Reporter 0.7.9 (Compomics; *http://compomics.github.io/*) (23). For protein/peptide identification, the MS/MS data were searched against the SwissProt human amino acid sequence database (Swiss-Prot Reviewed Homo Sapiens 2017.06; *http://www.uniprot.org/downloads*). Search parameters were the following: trypsin (no P rule), semispecific, 2 missed cleavages, deamidation of N and Q, oxidation of M, carbamidomethylation of C, isotope-coded cysteine-reactive tandem mass tag 6, precursor tolerance = 40.0 ppm, and fragment tolerance = 0.02 Da according to recommendations by Carvalho and coworkers (24). Various search engines integrated into Peptide Shaker *via* SearchGUI were used (Comet, MS Amanda, Tide, X!Tandem, MyriMatch, OMSSA, MS-GF$^+$) (25). Other details were the same as we previously described (14).

Kyoto Encyclopedia of Genes and Genomes pathways analysis

From the LC-MS/MS data, peptides that were altered upon Glrx overexpression (cutoff 1.3-fold) were analyzed by the Kyoto Encyclopedia of Genes and Genomes (KEGG) pathway using WebGestalt (*www.webgestalt.org/2013*).

Statistical analysis

All group data are expressed as means ± SEM. Statistical analysis comparing 2 groups was carried out using the 2-tailed, unpaired Student's *t* test. Analysis of more than 2 groups was performed by 1-way ANOVA followed by Tukey's *post hoc* comparison test. Repeated measure 1-way ANOVA analyzed sequential measurements. All analyses were carried out using Prism 7 software (GraphPad Software, La Jolla, CA, USA). A value of $P < 0.05$ was considered significant.

RESULTS

EC-specific Glrx overexpression impairs EC migration *in vivo*

EC-Glrx TG mice express a tTA, which binds to the tetracycline operating element, and induces expression of the FLAG-Glrx transgene. Withdrawal of DOX induced the expression of FLAG-tagged Glrx (**Fig. 1*A***).

Western blot analysis detected FLAG-tagged Glrx above endogenous Glrx at ~16 kDa) (Fig. 1*B*). FLAG and isolectin B4 staining—a specific molecular marker for EC—colocalized in the ECs of the skeletal muscle section (Fig. 1*C*). To examine EC migration in EC-Glrx TG mice, we subcutaneously injected Matrigel into mice and measured the hemoglobin content of the Matrigel as a surrogate marker for vascularization after 2 wk. Significant amounts of hemoglobin accumulated in Matrigel supplemented with VEGF, indicating ECs migrated into the Matrigel plug and formed functional blood-containing vessels. However, transgenic Glrx significantly impaired vascularization in mice (Fig. 1*D*). The representative photos show VEGF-treated Matrigel plugs removed from mice. CD31 staining demonstrates vascularity in Matrigel plugs from control mice (red arrows) but we barely detected CD31-positive cells in plugs from EC-Glrx TG mice. These data suggest that EC-specific Glrx overexpression suppresses EC migration and vessel formation *in vivo*.

EC-specific Glrx overexpression impairs ischemic angiogenesis

To examine the effects of EC-specific Glrx overexpression on ischemic angiogenesis, we performed hind limb ischemia surgery and analyzed blood flow recovery using Laser Doppler. After the surgery, it was evident by 7 d postsurgery that the EC-Glrx TG mice had significantly impaired recovery compared with the control group (**Fig. 2*A*, *B***). Also, some EC-Glrx TG mice developed necrotic limbs (Fig. 2*C*) and were euthanized according to the necrosis level, lowering the limb survival rate in this group (Fig. 2*D*). These results indicate that EC-specific Glrx overexpression impairs ischemic limb angiogenesis.

EC-specific Glrx overexpression impairs tumor angiogenesis but promotes tumor growth

Next, we investigated whether EC-specific Glrx overexpression impairs tumor angiogenesis in the host mouse. We implanted B16F0 melanoma cells subcutaneously into control and EC-Glrx TG mice to assess tumor growth and vascularization. Tumors from EC-Glrx TG mice had significantly decreased EC-specific markers CD31 (**Fig. 3*A*, *C***) and isolectin B4 (Fig. 3*B*, *D*) staining areas. Gene expression of Flt1 (VEGF receptor 1) was markedly lower (Supplemental Fig. S1, $P < 0.05$) and kinase insert domain receptor (Kdr; VEGF receptor 2) showed a trend of lower expression levels in tumors from EC-Glrx TG mice. Our data indicate that EC-specific Glrx overexpression impairs tumor angiogenesis in mice, and we anticipated tumor growth inhibition. However, B16F0 tumors from EC-Glrx TG mice showed a significant increase in weight and volume (**Fig. 4*A***). The mean ± SE tumor weight was 1229 ± 202 mg for EC-Glrx TG ($n = 8$) and 667 ± 160 mg for control mice ($n = 12$; $P < 0.05$).

Tumor cells may form vessel-like structures

Because tumors need sufficient blood perfusion to support cell growth and proliferation, non–EC-derived capillaries must supply the tumors in EC-Glrx TG mice. Reports indicated that tumor cells might acquire an EC-like phenotype and form vessels. This phenomenon, referred to as vasculogenic (or vascular) mimicry, was initially identified in aggressive human melanoma (20, 26). Immunohistochemistry of the EC marker CD31 in tumor sections showed blood-containing vessel-like structures surrounded by tumor cells without CD31-positive ECs (black arrows) as well as EC-surrounded lumina (red arrows) (Fig. 4*B*). To further distinguish vessels with or without EC, we injected a fluorescent-conjugated dextran dye (red) and stained EC for fluorescent-tagged CD31 antibody (green) (Fig. 4*C*). Using this method, we identified EC-lined vessels by colocalization of the dextran-conjugated dye and CD31 (yellow overlays) and vessels without ECs by the red dye-filled lumina (white arrows). Capillary lumina without EC appeared more frequently in tumors from EC-Glrx TG mice compared with control mice. In CD31-stained tumor sections, we found EC-deficient vessels in 4 out of 6 tumors examined from EC-Glrx TG mice, whereas only 1 out of 6 tumors examined from control mice contained EC-deficient vessels.

Hypoxia-induced VEGF may stimulate B16F0 tumor growth and vessel formation

Inadequate tumor angiogenesis due to attenuated EC migration from the host may render the tumor hypoxic. Indeed, tumors from EC-Glrx TG mice had markedly elevated VEGF protein levels (**Fig. 5*A***): EC-Glrx TG 494 ± 84 ng/mg ($n = 8$), control 299 ± 41 ng/mg ($n = 12$) ($P < 0.05$), which suggested activation of HIF-1 in the tumors of EC-Glrx TG mice. Accordingly, the immediate surroundings of larger vessels lacked HIF-1α expression, whereas tumors from EC-Glrx TG mice expressed it more diffusely, consistent with decreased vascularity and increased hypoxia (Fig. 5*B*).

To examine the impact of hypoxia on vascular-like structure formation by tumor cells, we performed an *in vitro* tube formation assay using B16F0 cells on Matrigel. Tumor cells formed tube-like structures more prominently under hypoxia (1% O_2) for 6 h *vs.* 20% O_2 (Fig. 5*C*). Hypoxia-exposed cells formed significantly longer networks with more intersections or branching points. These data support the hypothesis that hypoxic tumor cells can form channels and capillary-like structures, even in the absence of ECs. Furthermore, we tested the extent to which VEGF stimulates *in vitro* B16F0 tumor cell proliferation and tube formation. VEGF (2 and 5 ng/ml) stimulated B16F0 cell proliferation in a concentration-dependent manner (Fig. 5*D*) but failed to induce tumor cell network formation (Supplemental Fig. S3).

Identification of *S*-glutathionylated proteins regulated by Glrx in ECs

Glrx overexpression may influence protein *S*-glutathionylation, a reversible thiol modification that alters cell signaling pathways (4). To examine the protein *S*-glutathionylation regulated by Glrx in ECs, we performed a cysteine thiol labeling assay combined with mass spectrometric analysis as previously reported (14). We used a multiplex labeling approach with thiol-reactive tandem mass tags to identify reversibly modified protein cysteines on a site-specific basis for each condition. We only considered peptides and proteins that changed *S*-glutathionylation more than 1.3-fold when Glrx was overexpressed and submitted these proteins to KEGG pathway analysis. Supplemental Table S1 lists all pathway-assigned peptides. According to our pathway analysis, Glrx regulates cytoskeletal signaling molecules such as ACTB, Ras-related C3 botulinum toxin substrate 2 (RAC2), and thrombospondin (THBS1), all of which participate in angiogenesis. Compared with previous reports, we obtained similar results that Glrx-mediated deglutathionylation promotes ACTB polymerization (27), activates Rac, and decreases endothelial permeability (10). Thus, Glrx consistently activates mechanisms that inhibit EC migration and angiogenesis. Our analysis also showed changes in metabolic enzymes such as aldehyde dehydrogenase (ALDH2) and pyruvate kinase (PKM2) (**Fig. 6** and **Table 1**).

DISCUSSION

Increasing evidence shows that oxidants transduce redox signaling by reversible post-translational protein thiol modifications (4, 12). Protein *S*-glutathionylation, the formation of GSH adducts that is reversed by Glrx, occurs as a cysteine modification when cellular GSH is abundant. Thus, Glrx regulates cytoskeletal assembly (27, 28), apoptosis (29), fibrosis (30), EC barrier (10), and transcriptional pathways, including NF-κB (9, 31–33) and HIF-1α (11). We have shown that Glrx overexpression inhibits EC migration and ischemic limb revascularization (9). In this report, we generated mice overexpressing Glrx in an EC-specific manner and tested the effects on vascularization. EC- Glrx TG inhibited both ischemic limb vascularization and tumor angiogenesis. The mass spectrometry data indicated that multiple proteins relating to the angiogenesis pathway have reversible thiol modifications regulated by Glrx in EC. As it is known that protein phosphorylation transduces angiogenic signaling, our findings suggest a critical role for *S*-glutathionylation in EC in controlling angiogenic responses to ischemia.

In our B16F0 tumor implantation model, we found that EC-Glrx TG promoted tumor growth despite inhibited EC-derived angiogenesis. Reports show that aggressive tumor cells, including melanoma, form tube-like structures independent of EC-mediated angiogenesis, a phenomenon which is referred to as vasculogenic mimicry (recently called vascular mimicry). The presence of EC-independent microcirculation likely correlates with a poor cancer prognosis (34). We could detect blood cell–containing lumina without EC marker CD31 in the tumors from EC-Glrx TG mice more frequently than control mice, which indicates that tumor cell–derived vascular channels may support tumor growth when EC-dependent angiogenesis is inhibited. Hypoxia is a factor that promotes vasculogenic mimicry and tumor growth (35–38). We confirmed that B16F0 cells formed a network structure under the hypoxic condition. In EC-Glrx TG mice, tumors may become more hypoxic because of inhibited angiogenesis from the host. VEGF

protein levels were higher in tumors in EC-Glrx TG mice compared with those in control mice, which is indicative of a more hypoxic tumor microenvironment. Also, we confirmed that VEGF-A stimulated B16F0 tumor proliferation. Taken together, hypoxia-induced vasculogenic mimicry may support blood supply and tumor growth despite the antiangiogenic effects of EC-specific Glrx overexpression. Increased VEGF *per se* stimulates B16F0 cell proliferation (**Fig. 7**).

VEGF-A has been considered as a stimulatory factor of vasculogenic mimicry (34) and shown to promote vasculogenic mimicry–associated genes in ovarian carcinoma cells (39). We tested VEGF (5–50 ng/ml) on B16F0 but could not demonstrate its stimulation of tumor cell network formation. Recent studies demonstrate that inhibiting VEGF-A increases cancer stem cell–like population (40) and promotes vasculogenic mimicry in melanoma (41). Furthermore, anti–VEGF-A did not inhibit endothelial differentiation of cancer stem cells ($CD133^+$) (42). Therefore, VEGF-A may not promote vasculogenic mimicry directly, although hypoxia following antiangiogenic treatment may promote vasculogenic mimicry and tumor growth. HIF-1α activation increases breast cancer stem cells by regulation of the β-catenin pathway (40).

Since the original report described human melanoma (20), numerous published reports have characterized vasculogenic mimicry (34, 43, 44). We examined the expression of genes that may be associated with vasculogenic mimicry, including cadherin 5 (VEcad) (45), Flt1 (46), EPH receptor A2 (47), and neuropilin 1 (48), but found no significant increases in EC-Glrx TG tumors *vs.* control tumors (Supplemental Fig. S1). Interestingly, Glrx expression in the tumors of EC-Glrx TG mice was significantly lower than in control tumors. Despite Glrx overexpression in ECs, the hypoxic condition may suppress Glrx expression in the tumor cells. The lower Glrx expression may contribute to *S*-glutathionylation of HIF-1α, which stabilizes and activates HIF-1α in the tumor (11). A recent report also showed that hypoxia increased *S*-glutathionylation and stabilization of HIF-1α in colon cancer cells (49), suggesting that hypoxia and decreased Glrx expression enhanced HIF-1α activation.

One potential mechanism to support tumor growth in EC-Glrx TG mice is that Glrx overexpressing ECs may secrete cytokines or factors that influence tumor growth. Because Glrx can activate the NF-κB pathway (9, 33), we measured cytokine levels including IL-6 and C-C motif chemokine ligand 2 in the tumors, speculating that ECs may secrete higher levels of cytokines by Glrx overexpression. However, we did not find a significant difference (Supplemental Fig. S2) in the tumors. Glrx regulates protein function by reversing *S*-glutathionylation of protein thiols. There is still a possibility that EC-Glrx overexpression changes protein secretion from ECs and modifies tumor microenvironment.

Furthermore, we performed a mass spectrometric analysis to screen for *S*-glutathionylated proteins regulated by Glrx in EC. The data indicate that Glrx substrates in ECs are not only angiogenesis-related proteins, such as focal adhesion molecules and cytoskeletal proteins, but also include proteins involved in metabolic pathways. Among the proteins in which Glrx regulates thiol modification (Supplemental Table S1), some proteins can be secreted or released from ECs. For instance, endoglin (50), fibronectin (51), serpins (52), thrombospondin (53), and connective tissue growth factor (54) can be released in soluble form from ECs and regulate angiogenesis and the tumor microenvironment. Glrx-regulated redox-sensitive cysteines may modulate the release or function of these soluble factors. Endoglin (CD105), known as a regulatory receptor for TGF-β and predominantly expressed in ECs, contains a large extracellular domain. The cleaved form soluble-endoglin increases in the plasma of patients with cancer (55). We found that Cys^{372} and Cys^{384} of human endoglin in the soluble part of the extracellular domain are modified by Glrx. However, we need further studies to elucidate how *S*-glutathionylation of these cysteines may cause conformational changes of endoglin or alter TGF-β signaling.

Another interesting finding is Cys oxidation of PKM2. PKM2 is an enzyme in the glycolysis pathway and produces pyruvate and ATP. Oxidants inhibit PKM2 *via* Cys^{358} (56), and we found Cys^{358} is reversibly modified by Glrx. In response to oxidative inhibition of PKM2, glucose flux generates reducing potential *via* pentose phosphate pathway overcoming oxidative stress (56). Thus, Glrx may prevent Cys^{358} oxidation, activate PKM2, and promote an oxidative condition.

There are some limitations to this study. We assessed B16F0 tumor growth only at a single time point, but the time course of tumor growth may provide additional insights into the regulation of EC-angiogenesis and vascular mimicry. Also, we did not confirm factors that Glrx overexpressing EC may release directly

to stimulate vasculogenic mimicry and tumor growth. It also remains unclear whether vasculogenic mimicry is a general mechanism to circumvent EC-angiogenesis or specific to certain tumors, such as melanoma. We need extensive future work to elucidate the exact mechanisms that enable tumor cells to acquire a vascular feature. We speculate that tumors with a lower potential of vasculogenic mimicry may respond differently to inhibition of EC-angiogenesis.

In summary, up-regulated expression of Glrx in EC inhibited mouse ischemic limb vascularization and tumor angiogenesis but promoted subcutaneous melanoma tumor growth. Antiangiogenic ECs may cause hypoxia in the tumor and stimulate vascular channel formation by tumor cells. Our study implies that tumors have a mechanism to overcome antiangiogenic therapies, and the host with poor ischemic vascularization is not necessarily associated with slower tumor growth.

ACKNOWLEDGMENTS

The authors thank Dr. Nader Rahimi for advice, and Dominique Croteau for editing the manuscript (both from the Boston University School of Medicine). The authors also thank Professor Stephen Chlopicki and his laboratory members (Jagiellonian Centre for Experimental Therapeutics, Krakow, Poland) for helpful advice, and the Analytical Instrumentation Core at Boston University Medical Campus for their service. This research was supported by U.S. National Institutes of Health (NIH)/National Heart, Lung, and Blood Institute (NHLBI) Grant R01 HL133013 (to R.M.), postdoctoral training Grant T32 HL70024 (to B.F.), R37 HL104017 (to R.A.C.), and contract HHSN268201000031C (to C.E.C.); NIH/National Institute on Aging Grant R03 AG051857 (to R.M.); NIH/National Center for Advancing Translational Sciences Grant 1UL1 TR001430 (to M.M.B. and R.M.); NIH/National Institute of Diabetes and Digestive and Kidney Diseases Grant R01 DK103750 (to M.M.B.); and American Heart Association Grant 16GRNT27660006 (to M.M.B.). The authors declare no conflicts of interest.

Glossary

ACTB	β-actin
ALDH2	aldehyde dehydrogenase
DOX	doxycycline
EC	endothelial cell
EC-Glrx TG	EC-specific glutaredoxin-1 transgenic
Flt1	fms-related tyrosine kinase 1
Glrx	glutaredoxin-1
GSH	glutathione
HCMVEC	human cardiac microvascular EC
HIF	hypoxia-inducible factor
KEGG	Kyoto Encyclopedia of Genes and Genomes
LC-MS/MS	liquid chromatography-tandem mass spectrometry
PKM2	pyruvate kinase
RAC	Ras-related C3 botulinum toxin substrate
tTA	tetracycline transactivator
VE	vascular endothelial
VEcad	VE-cadherin

Footnotes

This article includes supplemental data. Please visit *http://www.fasebj.org* to obtain this information.

AUTHOR CONTRIBUTIONS

Y. Yura, Y. Watanabe, and R. Matsui designed the research; Y. Yura, B. S. H. Chong, R. D. Johnson, Y. Watanabe, Y. Tsukahara, B. Ferran, C. E. Murdoch, and J. B. Behring performed the research; Y. Yura, Y. Watanabe, B. S. H. Chong, M. M. Bachschmid, and R. Matsui analyzed the data; Y. M. W. Janssen-Heininger and R. A. Cohen provided research tools and support; M. E. McComb, C. E. Costello, and M. M. Bachschmid contributed to analytic tools and data interpretation; Y. Yura and R. Matsui wrote the paper; and all authors reviewed and edited the manuscript.

Supplementary Material

This article includes supplemental data. Please visit *http://www.fasebj.org* to obtain this information.

REFERENCES

1. Sundaresan M., Yu Z. X., Ferrans V. J., Irani K., Finkel T. (1995) Requirement for generation of H2O2 for platelet-derived growth factor signal transduction. Science 270, 296–299 [PubMed: 7569979]

2. Janssen-Heininger Y. M. W., Mossman B. T., Heintz N. H., Forman H. J., Kalyanaraman B., Finkel T., Stamler J. S., Rhee S. G., van der Vliet A. (2008) Redox-based regulation of signal transduction: principles, pitfalls, and promises. Free Radic. Biol. Med. 45, 1–17 [PMCID: PMC2453533] [PubMed: 18423411]

3. Schieber M., Chandel N. S. (2014) ROS function in redox signaling and oxidative stress. Curr. Biol. 24, R453–R462 [PMCID: PMC4055301] [PubMed: 24845678]

4. Pimentel D., Haeussler D. J., Matsui R., Burgoyne J. R., Cohen R. A., Bachschmid M. M. (2012) Regulation of cell physiology and pathology by protein S-glutathionylation: lessons learned from the cardiovascular system. Antioxid. Redox Signal. 16, 524–542 [PMCID: PMC3270052] [PubMed: 22010840]

5. Dalle-Donne I., Rossi R., Colombo G., Giustarini D., Milzani A. (2009) Protein S-glutathionylation: a regulatory device from bacteria to humans. Trends Biochem. Sci. 34, 85–96 [PubMed: 19135374]

6. Lamalice L., Le Boeuf F., Huot J. (2007) Endothelial cell migration during angiogenesis. Circ. Res. 100, 782–794 [PubMed: 17395884]

7. Adachi T., Weisbrod R. M., Pimentel D. R., Ying J., Sharov V. S., Schöneich C., Cohen R. A. (2004) S-Glutathiolation by peroxynitrite activates SERCA during arterial relaxation by nitric oxide. Nat. Med. 10, 1200–1207 [PubMed: 15489859]

8. Evangelista A. M., Thompson M. D., Weisbrod R. M., Pimental D. R., Tong X., Bolotina V. M., Cohen R. A. (2012) Redox regulation of SERCA2 is required for vascular endothelial growth factor-induced signaling and endothelial cell migration. Antioxid. Redox Signal. 17, 1099–1108 [PMCID: PMC3423867] [PubMed: 22472004]

9. Murdoch C. E., Shuler M., Haeussler D. J., Kikuchi R., Bearelly P., Han J., Watanabe Y., Fuster J. J., Walsh K., Ho Y. S., Bachschmid M. M., Cohen R. A., Matsui R. (2014) Glutaredoxin-1 up-regulation induces soluble vascular endothelial growth factor receptor 1, attenuating post-ischemia limb revascularization. J. Biol. Chem. 289, 8633–8644 [PMCID: PMC3961686] [PubMed: 24482236]

10. Han J., Weisbrod R. M., Shao D., Watanabe Y., Yin X., Bachschmid M. M., Seta F., Janssen-Heininger Y. M. W., Matsui R., Zang M., Hamburg N. M., Cohen R. A. (2016) The redox mechanism for vascular barrier dysfunction associated with metabolic disorders: glutathionylation of Rac1 in endothelial cells. Redox Biol. 9, 306–319 [PMCID: PMC5045950] [PubMed: 27693992]

11. Watanabe Y., Murdoch C. E., Sano S., Ido Y., Bachschmid M. M., Cohen R. A., Matsui R. (2016) Glutathione adducts induced by ischemia and deletion of glutaredoxin-1 stabilize HIF-1α and improve limb revascularization. Proc. Natl. Acad. Sci. USA 113, 6011–6016 [PMCID: PMC4889374] [PubMed: 27162359]

12. Matsui R., Watanabe Y., Murdoch C. E. (2017) Redox regulation of ischemic limb neovascularization - what we have learned from animal studies. Redox Biol. 12, 1011–1019 [PMCID: PMC5430575] [PubMed: 28505880]

13. Murdoch C., Muthana M., Coffelt S. B., Lewis C. E. (2008) The role of myeloid cells in the promotion of tumour angiogenesis. Nat. Rev. Cancer 8, 618–631 [PubMed: 18633355]

14. Behring J. B., Kumar V., Whelan S. A., Chauhan P., Siwik D. A., Costello C. E., Colucci W. S., Cohen R. A., McComb M. E., Bachschmid M. M. (2014) Does reversible cysteine oxidation link the Western diet to cardiac dysfunction? FASEB J. 28, 1975–1987 [PMCID: PMC4046179] [PubMed: 24469991]

15. Anathy V., Aesif S. W., Hoffman S. M., Bement J. L., Guala A. S., Lahue K. G., Leclair L. W., Suratt B. T., Cool C. D., Wargo M. J., Janssen-Heininger Y. M. (2014) Glutaredoxin-1 attenuates S-glutathionylation of the death receptor fas and decreases resolution of Pseudomonas aeruginosa pneumonia. Am. J. Respir. Crit. Care Med. 189, 463–474 [PMCID: PMC3977722] [PubMed: 24325366]

16. Limbourg A., Korff T., Napp L. C., Schaper W., Drexler H., Limbourg F. P. (2009) Evaluation of postnatal arteriogenesis and angiogenesis in a mouse model of hind-limb ischemia. Nat. Protoc. 4, 1737–1746 [PubMed: 19893509]

17. Auerbach R., Lewis R., Shinners B., Kubai L., Akhtar N. (2003) Angiogenesis assays: a critical overview. Clin. Chem. 49, 32–40 [PubMed: 12507958]

18. Tomayko M. M., Reynolds C. P. (1989) Determination of subcutaneous tumor size in athymic (nude) mice. Cancer Chemother. Pharmacol. 24, 148–154 [PubMed: 2544306]

19. Dunleavey J. M., Xiao L., Thompson J., Kim M. M., Shields J. M., Shelton S. E., Irvin D. M., Brings V. E., Ollila D. W., Brekken R. A., Dayton P. A., Melero-Martin J. M., Dudley A. C. (2014) Vascular channels formed by subpopulations of PECAM1+ melanoma cells. Nat. Commun. 5, 5200 [PMCID: PMC4261234] [PubMed: 25335460]

20. Maniotis A. J., Folberg R., Hess A., Seftor E. A., Gardner L. M., Pe'er J., Trent J. M., Meltzer P. S., Hendrix M. J. (1999) Vascular channel formation by human melanoma cells *in vivo* and *in vitro*: vasculogenic mimicry. Am. J. Pathol. 155, 739–752 [PMCID: PMC1866899] [PubMed: 10487832]

21. Wild R., Ramakrishnan S., Sedgewick J., Griffioen A. W. (2000) Quantitative assessment of angiogenesis and tumor vessel architecture by computer-assisted digital image analysis: effects of VEGF-toxin conjugate on tumor microvessel density. Microvasc. Res. 59, 368–376 [PubMed: 10792968]

22. Bondjers C., Kalén M., Hellström M., Scheidl S. J., Abramsson A., Renner O., Lindahl P., Cho H., Kehrl J., Betsholtz C. (2003) Transcription profiling of platelet-derived growth factor-B-deficient mouse embryos identifies RGS5 as a novel marker for pericytes and vascular smooth muscle cells. Am. J. Pathol. 162, 721–729 [PMCID: PMC1868109] [PubMed: 12598306]

23. Vaudel M., Burkhart J. M., Zahedi R. P., Oveland E., Berven F. S., Sickmann A., Martens L., Barsnes H. (2015) PeptideShaker enables reanalysis of MS-derived proteomics data sets. Nat. Biotechnol. 33, 22–24 [PubMed: 25574629]

24. Carvalho P. C., Lima D. B., Leprevost F. V., Santos M. D., Fischer J. S., Aquino P. F., Moresco J. J., Yates J. R., III, Barbosa V. C. (2016) Integrated analysis of shotgun proteomic data with PatternLab for proteomics 4.0. Nat. Protoc. 11, 102–117 [PMCID: PMC5722229] [PubMed: 26658470]

25. Barsnes H., Vaudel M. (2018) SearchGUI: a highly adaptable common interface for proteomics search and de novo engines. J. Proteome Res. 17, 2552–2555 [PubMed: 29774740]

26. Folberg R., Hendrix M. J. C., Maniotis A. J. (2000) Vasculogenic mimicry and tumor angiogenesis. Am. J. Pathol. 156, 361–381 [PMCID: PMC1850026] [PubMed: 10666364]

27. Wang J., Boja E. S., Tan W., Tekle E., Fales H. M., English S., Mieyal J. J., Chock P. B. (2001) Reversible glutathionylation regulates actin polymerization in A431 cells. J. Biol. Chem. 276, 47763–47766 [PubMed: 11684673]

28. Bachschmid M. M., Xu S., Maitland-Toolan K. A., Ho Y. S., Cohen R. A., Matsui R. (2010) Attenuated cardiovascular hypertrophy and oxidant generation in response to angiotensin II infusion in glutaredoxin-1 knockout mice. Free Radic. Biol. Med. 49, 1221–1229 [PMCID: PMC2930025] [PubMed: 20638471]

29. Anathy V., Aesif S. W., Guala A. S., Havermans M., Reynaert N. L., Ho Y. S., Budd R. C., Janssen-Heininger Y. M. (2009) Redox amplification of apoptosis by caspase-dependent cleavage of glutaredoxin 1 and S-glutathionylation of Fas. J. Cell Biol. 184, 241–252 [PMCID: PMC2654302] [PubMed: 19171757]

30. Anathy V., Lahue K. G., Chapman D. G., Chia S. B., Casey D. T., Aboushousha R., van der Velden J. L. J., Elko E., Hoffman S. M., McMillan D. H., Jones J. T., Nolin J. D., Abdalla S., Schneider R., Seward D. J., Roberson E. C., Liptak M. D., Cousins M. E., Butnor K. J., Taatjes D. J., Budd R. C., Irvin C. G., Ho Y. S., Hakem R., Brown K. K., Matsui R., Bachschmid M. M., Gomez J. L., Kaminski N., van der Vliet A., Janssen-Heininger Y. M. W. (2018) Reducing protein oxidation reverses lung fibrosis. Nat. Med. 24, 1128–1135 [PMCID: PMC6204256] [PubMed: 29988126]

31. Reynaert N. L., Wouters E. F. M., Janssen-Heininger Y. M. W. (2007) Modulation of glutaredoxin-1 expression in a mouse model of allergic airway disease. Am. J. Respir. Cell Mol. Biol. 36, 147–151 [PMCID: PMC1899315] [PubMed: 16980552]

32. Shelton M. D., Kern T. S., Mieyal J. J. (2007) Glutaredoxin regulates nuclear factor kappa-B and intercellular adhesion molecule in Müller cells: model of diabetic retinopathy. J. Biol. Chem. 282, 12467–12474 [PubMed: 17324929]

33. Gorelenkova Miller O., Behring J. B., Siedlak S. L., Jiang S., Matsui R., Bachschmid M. M., Zhu X., Mieyal J. J. (2016) Upregulation of glutaredoxin-1 activates microglia and promotes neurodegeneration: implications for Parkinson's disease. Antioxid. Redox Signal. 25, 967–982 [PMCID: PMC5175443] [PubMed: 27224303]

34. Delgado-Bellido D., Serrano-Saenz S., Fernández-Cortés M., Oliver F. J. (2017) Vasculogenic mimicry signaling revisited: focus on non-vascular VE-cadherin. Mol. Cancer 16, 65 [PMCID: PMC5359927] [PubMed: 28320399]

35. Hendrix M. J. C., Seftor R. E., Seftor E. A., Gruman L. M., Lee L. M., Nickoloff B. J., Miele L., Sheriff D. D., Schatteman G. C. (2002) Transendothelial function of human metastatic melanoma cells: role of the microenvironment in cell-fate determination. Cancer Res. 62, 665–668 [PubMed: 11830517]

36. Sun B., Zhang D., Zhang S., Zhang W., Guo H., Zhao X. (2007) Hypoxia influences vasculogenic mimicry channel formation and tumor invasion-related protein expression in melanoma. Cancer Lett. 249, 188–197 [PubMed: 16997457]

37. Ma J. L., Han S. X., Zhu Q., Zhao J., Zhang D., Wang L., Lv Y. (2011) Role of Twist in vasculogenic mimicry formation in hypoxic hepatocellular carcinoma cells *in vitro*. Biochem. Biophys. Res. Commun. 408, 686–691 [PubMed: 21539816]

38. Fernández-Barral A., Orgaz J. L., Gomez V., del Peso L., Calzada M. J., Jiménez B. (2012) Hypoxia negatively regulates antimetastatic PEDF in melanoma cells by a hypoxia inducible factor-independent, autophagy dependent mechanism. PLoS One 7, e32989 [PMCID: PMC3311626] [PubMed: 22457728]

39. Wang J.-Y., Sun T., Zhao X. L., Zhang S. W., Zhang D. F., Gu Q., Wang X. H., Zhao N., Qie S., Sun B. C. (2008) Functional significance of VEGF-a in human ovarian carcinoma: role in vasculogenic mimicry. Cancer Biol. Ther. 7, 758–766 [PubMed: 18376140]

40. Conley S. J., Gheordunescu E., Kakarala P., Newman B., Korkaya H., Heath A. N., Clouthier S. G., Wicha M. S. (2012) Antiangiogenic agents increase breast cancer stem cells via the generation of tumor hypoxia. Proc. Natl. Acad. Sci. USA 109, 2784–2789 [PMCID: PMC3286974] [PubMed: 22308314]

41. Schnegg C. I., Yang M. H., Ghosh S. K., Hsu M.-Y. (2015) Induction of vasculogenic mimicry overrides VEGF-A silencing and enriches stem-like cancer cells in melanoma. Cancer Res. 75, 1682–1690 [PMCID: PMC4401656] [PubMed: 25769726]

42. Wang R., Chadalavada K., Wilshire J., Kowalik U., Hovinga K. E., Geber A., Fligelman B., Leversha M., Brennan C., Tabar V. (2010) Glioblastoma stem-like cells give rise to tumour endothelium. Nature 468, 829–833 [PubMed: 21102433]

43. Hendrix M. J. C., Seftor E. A., Seftor R. E., Chao J. T., Chien D. S., Chu Y. W. (2016) Tumor cell vascular mimicry: novel targeting opportunity in melanoma. Pharmacol. Ther. 159, 83–92 [PMCID: PMC4779708] [PubMed: 26808163]

44. Sun B., Zhang D., Zhao N., Zhao X. (2017) Epithelial-to-endothelial transition and cancer stem cells: two cornerstones of vasculogenic mimicry in malignant tumors. Oncotarget 8, 30502–30510 [PMCID: PMC5444760] [PubMed: 27034014]

45. Hendrix M. J. C., Seftor E. A., Meltzer P. S., Gardner L. M., Hess A. R., Kirschmann D. A., Schatteman G. C., Seftor R. E. (2001) Expression and functional significance of VE-cadherin in aggressive human melanoma cells: role in vasculogenic mimicry. Proc. Natl. Acad. Sci. USA 98, 8018–8023 [PMCID: PMC35460] [PubMed: 11416160]

46. Frank N. Y., Schatton T., Kim S., Zhan Q., Wilson B. J., Ma J., Saab K. R., Osherov V., Widlund H. R., Gasser M., Waaga-Gasser A. M., Kupper T. S., Murphy G. F., Frank M. H. (2011) VEGFR-1 expressed by malignant melanoma-initiating cells is required for tumor growth. Cancer Res. 71, 1474–1485 [PMCID: PMC3083845] [PubMed: 21212411]

47. Hess A. R., Seftor E. A., Gardner L. M., Carles-Kinch K., Schneider G. B., Seftor R. E., Kinch M. S., Hendrix M. J. (2001) Molecular regulation of tumor cell vasculogenic mimicry by tyrosine phosphorylation: role of epithelial cell kinase (Eck/EphA2). Cancer Res. 61, 3250–3255 [PubMed:

11309274]

48. Misra R. M., Bajaj M. S., Kale V. P. (2012) Vasculogenic mimicry of HT1080 tumour cells *in vivo*: critical role of HIF-1α-neuropilin-1 axis. PLoS One 7, e50153 [PMCID: PMC3504006] [PubMed: 23185562]

49. Jeon D., Park H. J., Kim H. S. (2018) Protein S-glutathionylation induced by hypoxia increases hypoxia-inducible factor-1α in human colon cancer cells. Biochem. Biophys. Res. Commun. 495, 212–216 [PubMed: 29113799]

50. Fonsatti E., Altomonte M., Nicotra M. R., Natali P. G., Maio M. (2003) Endoglin (CD105): a powerful therapeutic target on tumor-associated angiogenetic blood vessels. Oncogene 22, 6557–6563 [PubMed: 14528280]

51. Ingber D. E. (1990) Fibronectin controls capillary endothelial cell growth by modulating cell shape. Proc. Natl. Acad. Sci. USA 87, 3579–3583 [PMCID: PMC53945] [PubMed: 2333303]

52. Daniel A. E., Timmerman I., Kovacevic I., Hordijk P. L., Adriaanse L., Paatero I., Belting H. G., van Buul J. D. (2015) Plasminogen activator inhibitor-1 controls vascular integrity by regulating VE-cadherin trafficking. PLoS One 10, e0145684 [PMCID: PMC4694698] [PubMed: 26714278]

53. Huang T., Sun L., Yuan X., Qiu H. (2017) Thrombospondin-1 is a multifaceted player in tumor progression. Oncotarget 8, 84546–84558 [PMCID: PMC5663619] [PubMed: 29137447]

54. Ramazani Y., Knops N., Elmonem M. A., Nguyen T. Q., Arcolino F. O., van den Heuvel L., Levtchenko E., Kuypers D., Goldschmeding R. (2018) Connective tissue growth factor (CTGF) from basics to clinics. Matrix Biol. 68-69, 44–66 [PubMed: 29574063]

55. Nassiri F., Cusimano M. D., Scheithauer B. W., Rotondo F., Fazio A., Yousef G. M., Syro L. V., Kovacs K., Lloyd R. V. (2011) Endoglin (CD105): a review of its role in angiogenesis and tumor diagnosis, progression and therapy. Anticancer Res. 31, 2283–2290 [PubMed: 21737653]

56. Anastasiou D., Poulogiannis G., Asara J. M., Boxer M. B., Jiang J. K., Shen M., Bellinger G., Sasaki A. T., Locasale J. W., Auld D. S., Thomas C. J., Vander Heiden M. G., Cantley L. C., et al. (2011) Inhibition of pyruvate kinase M2 by reactive oxygen species contributes to cellular antioxidant responses. Science 334, 1278–1283 [PMCID: PMC3471535] [PubMed: 22052977]

Figures and Tables

Figure 1

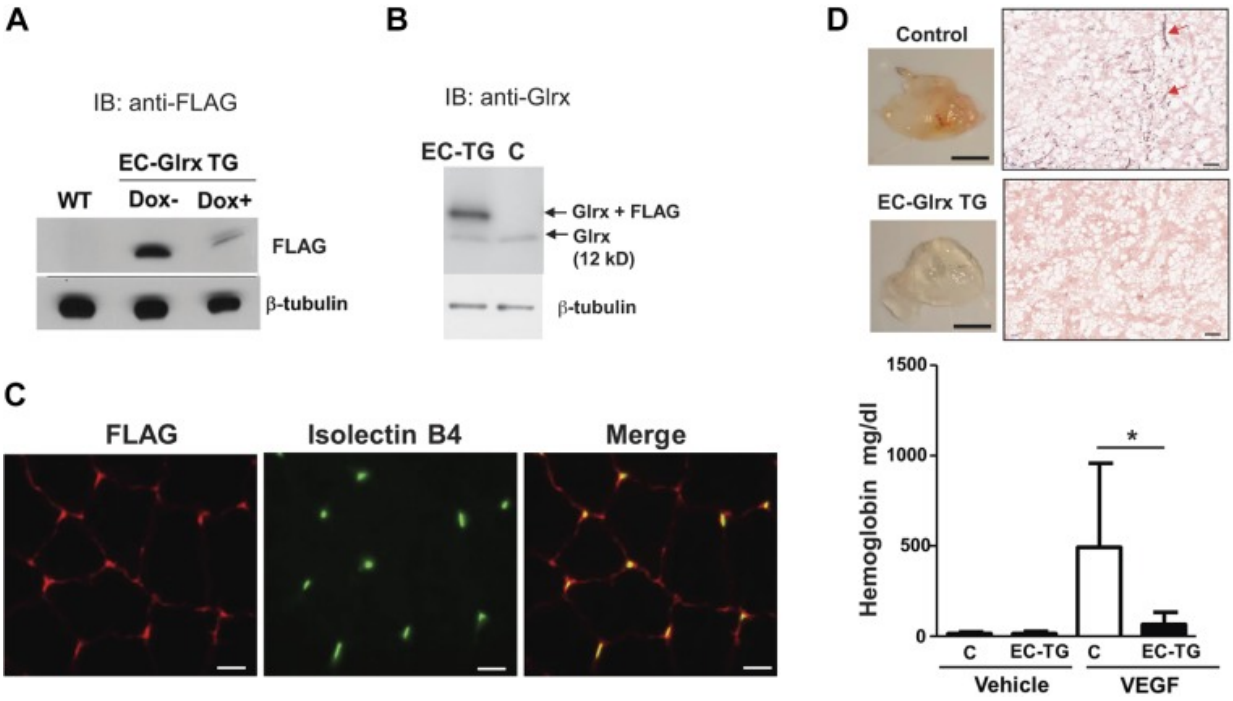

EC-specific Glrx overexpression impaired EC migration *in vivo*. *A*) Protein extracts from lungs in EC-Glrx TG mice with or without DOX were blotted and probed with antibodies directed against FLAG. *B*) Lung proteins from the control and EC-Glrx TG mice without DOX were blotted with the anti-Glrx antibody; the upper band indicates exogenous FLAG-Glrx, whereas the lower band indicates endogenous Glrx. *C*) FLAG-Glrx (red) colocalizes with the EC marker isolectin B4 (green) in cross sections of the gastrocnemius muscle. *D*) EC migration *in vivo* assay. Hemoglobin content in Matrigel plugs implanted subcutaneously in EC-Glrx TG (EC-TG) and control mice for 2 wk with or without VEGF ($n = 8$). *$P <$ 0.05. The photos show VEGF-containing Matrigel plugs (scale bars, 5 mm) and immunohistochemistry for CD31 (red arrows; scale bars, 100 μm) in the plugs from control (C) and EC-Glrx TG mice.

Figure 2

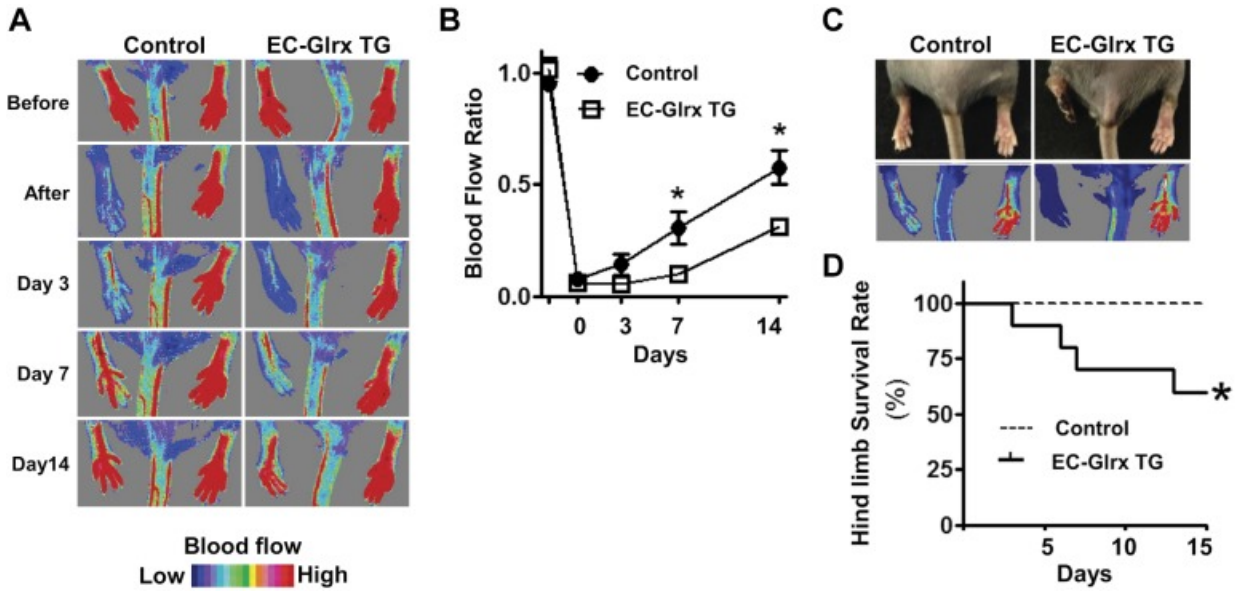

EC-specific Glrx overexpression impaired ischemic angiogenesis in mice. *A*) Blood flow after hind limb ischemia surgery, assessed by Laser Doppler. Representative photos show the blood flow recovery. *B*) EC-Glrx TG mice were compared with VEcad-tTA (single TG) or wild-type mice as control with quantitative serial assessment, $n = 8$ each. *C*) Representative photos show necrotic foot observed with EC-Glrx TG mice. *D*) Limb survival curve indicates that EC-Glrx TG mice had a higher incidence of necrotic legs. $^*P < 0.05$.

Figure 3

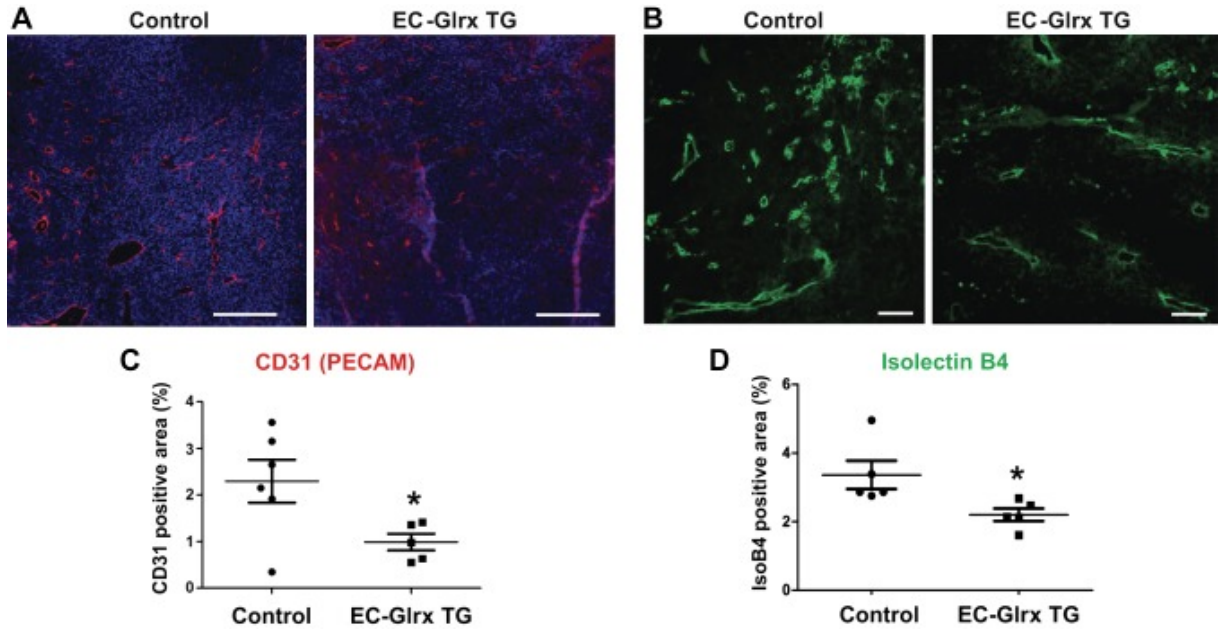

EC-specific Glrx overexpression impaired tumor angiogenesis. *A*) Vascularization of B16F0 tumors determined by immunofluorescent staining for CD31. Representative images of tumors with CD31 (red) and Hoechst 33342 (blue) from control and EC-Glrx TG tumors (scale bar, 500 μm). *B*) Representative photos to show isolectin B4 staining (green) in B16F0 tumors from control and EC-Glrx TG mice (scale bar, 200 μm). *C*) Relative CD31-positive area quantification from tumor section in *A* ($n = 6$). *D*) Relative isolectin B4–positive area quantification from tumor section from *B* ($n = 5$).

Figure 4

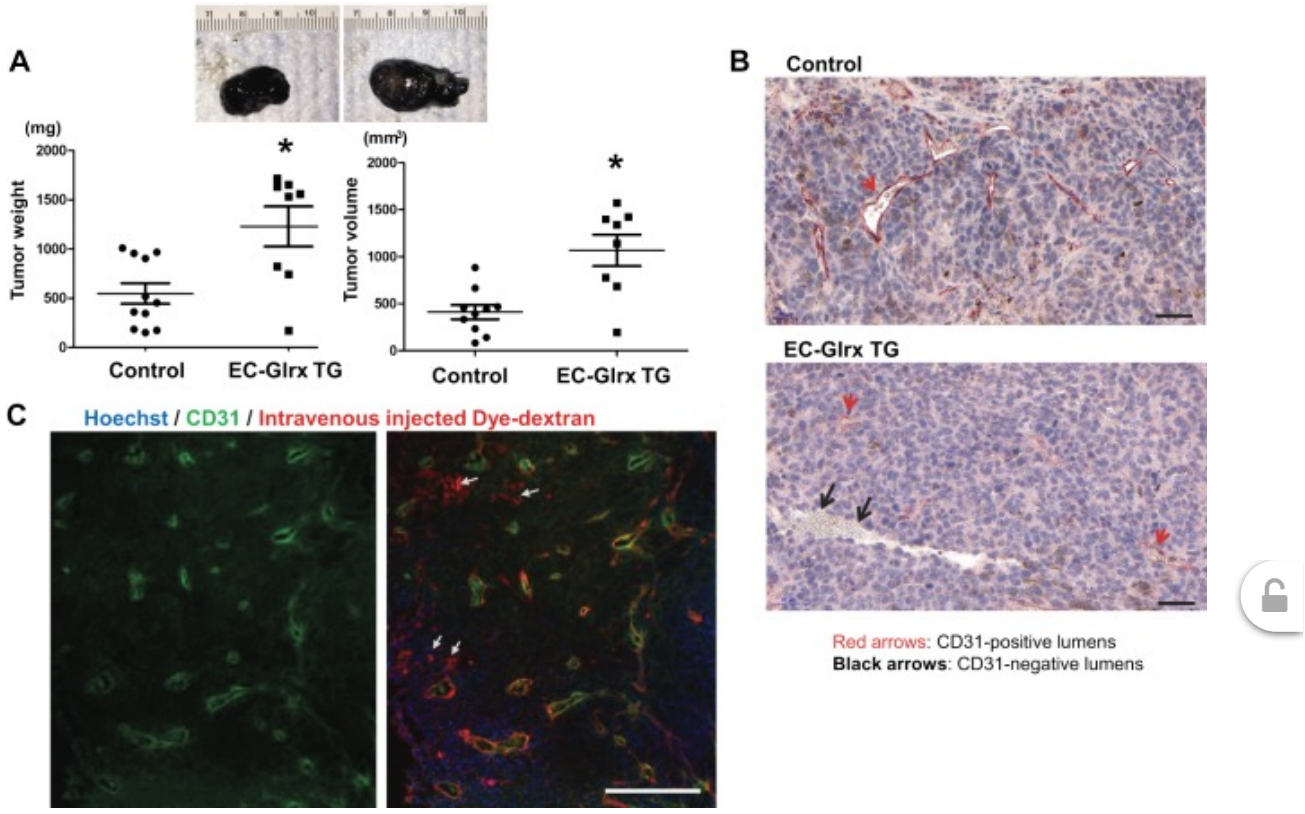

EC-specific Glrx overexpression promoted tumor growth and EC-independent tube formation in B16F0 tumors. *A*) B16F0 tumors from control and EC-Glrx TG mice, extracted after 2 wk of inoculation. Representative photos of tumors (top), and weight and volume assessments ($n = 8–12$). *$P < 0.05$. *B*) CD31 staining on the paraffin section of B16F0 tumors demonstrates EC-lining lumina (CD31-positive cells shown in red arrows) as well as blood cell–containing lumen without CD31 staining (shown by black arrows, mostly found in EC-Glrx TG tumors). Photos are representative sections of tumors from EC-Glrx TG and control mice (scale bars, 50 μm). *C*) Blood flow in a tumor without endothelium in Texas Red-labeled Dextran-injected EC-Glrx TG mouse. CD31 from tumor sections were stained in green (left). The merged photo (right) indicates dye-conjugated dextran in blood flow (red), CD31 in EC (green), and nuclear staining Hoechst 33342 (blue). White arrows point to Dextran-positive CD31-negative areas (scale bar, 500 μm).

Figure 5

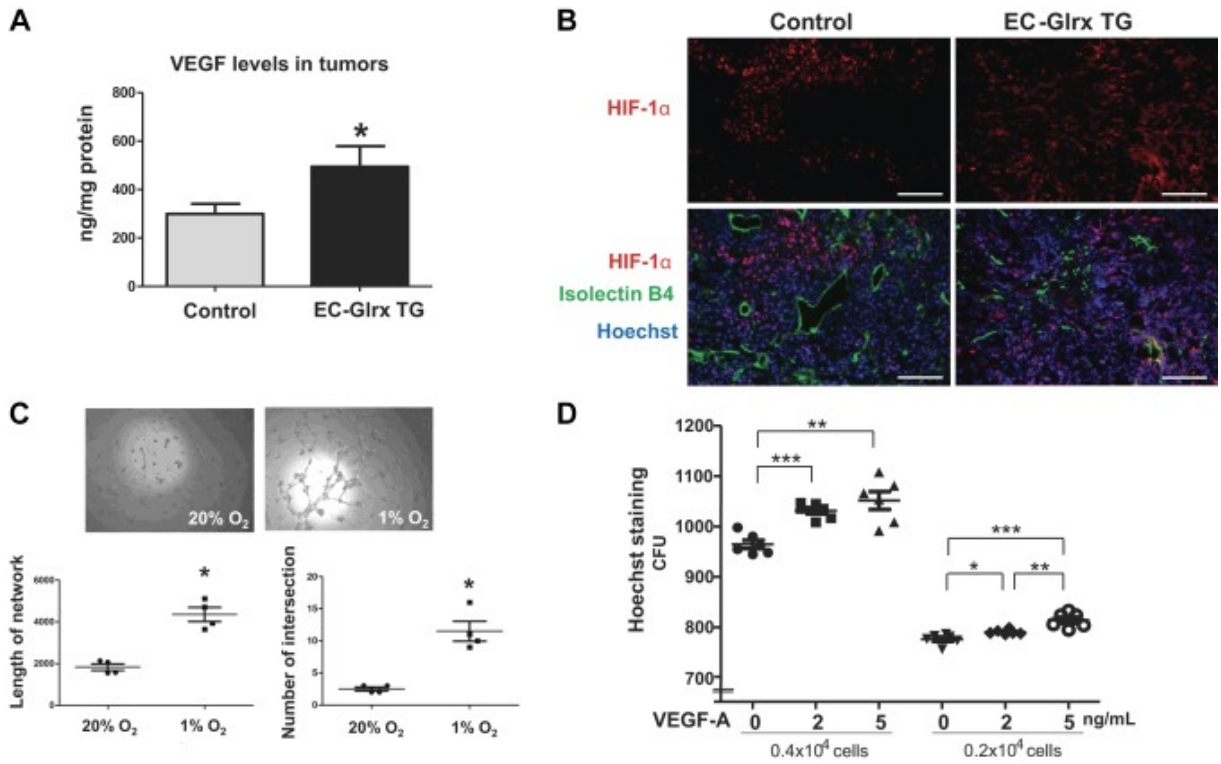

Hypoxia may stimulate B16F0 tumor growth and EC-independent vessel formation. *A*) VEGF levels in the tumor assessed by ELISA. *$P < 0.05$. *B*) Immunoflurescence for HIF-1a (red), isolectin B4 (green), and Hoechst 33342 (blue) of B16 tumors (scale bars, 100 μm). *C*) Capillary tube formation of B16F0 cells on Matrigel assessed <1 or 20% O_2. Intersections were determined by recording the number of connections between 2 or more capillary-like structures per field. The length of the tube was quantified by the sum of total tube length per field. Images of B16F0 cells from both 20 and 1% O_2 show that hypoxia (6 h) increased tube formation ($n = 4$ wells/condition). *$P < 0.05$. Similar results were observed at least in 3 different experiments. *D*) Two different density of cells were tested to study the effect of VEGF (2–5 ng/ml) on B16F0 cell proliferation. Hoechst 33342 nuclear staining was assessed after 24 h (6 wells each). *$P < 0.05$, **$P < 0.01$, ***$P < 0.001$. The representative data are shown from similar experiments repeated 3 times.

Figure 6

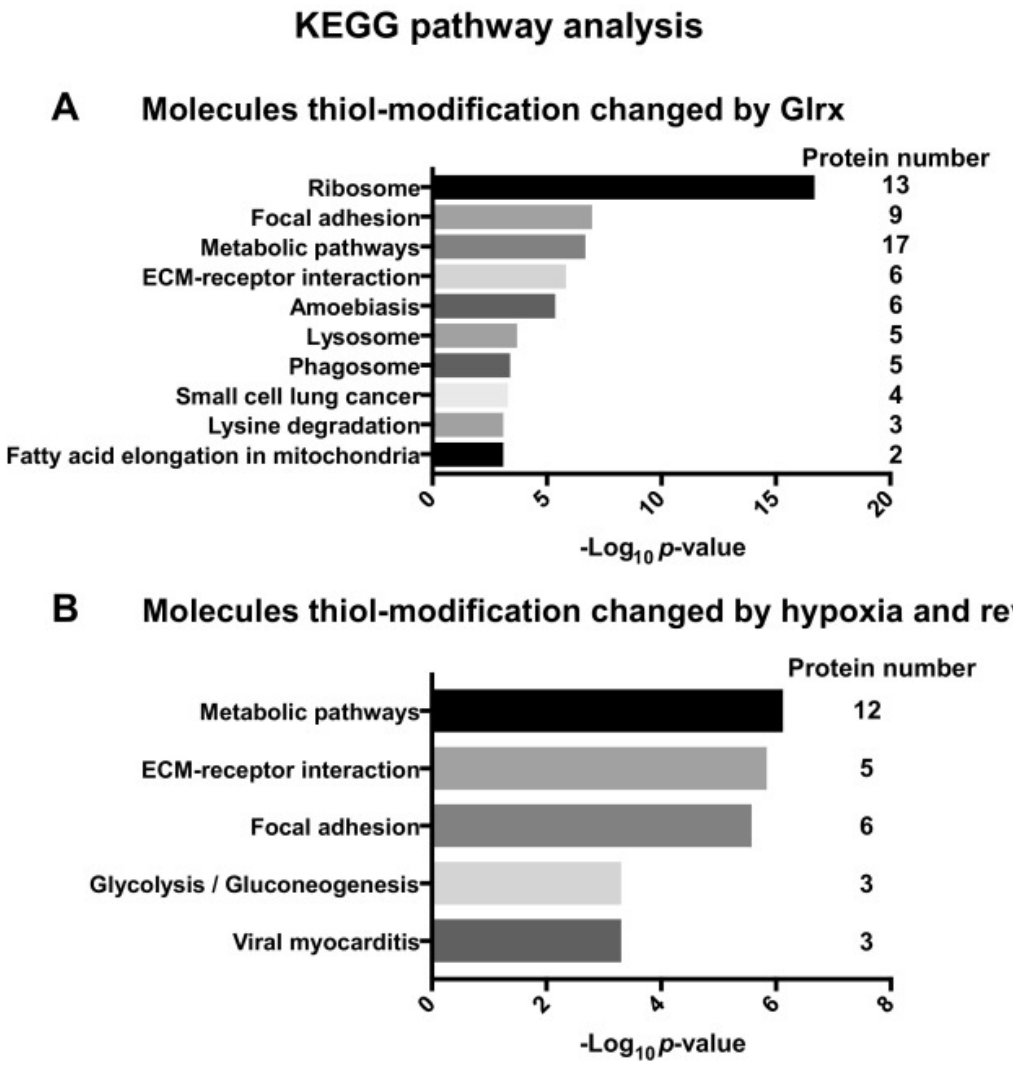

S-glutathionylated proteins regulated by Glrx in EC. KEGG pathway analysis of reversibly thiol-modified proteins using WebGestalt. Adenoviral Glrx or LacZ overexpressing HCMVECs were exposed to hypoxia for 24 h, and proteins were labeled as described in Materials and Methods. All proteins in which thiol modifications were reversed by Glrx overexpression (cutoff: 1.3-fold) are summarized in Supplemental Table S1. The pathways exhibiting significant changes in normoxia (*A*) or hypoxia (*B*) are shown. Table 1 lists the proteins by pathway regulated through Glrx in hypoxia.

TABLE 1

Proteins whose thiol modifications were changed by hypoxia and reversed by Glrx (KEGG pathway analysis)

KEGG pathway/ID	Protein symbol	UniProtKB	Protein name
Metabolic pathways ID: 01100	HPRT1	P00492	Hypoxanthin-guanine phosphoribosyltransferase 1
	ALDH2	P05091	Aldehyde dehydrogenase 2, mitochondrial
	MT-CO2	P00403	Cytochrome *c* oxidase subunit 2
	DCXR	Q7Z4W1	Dicarbonyl/L-xylulose reductase
	DUT	P33316	Deoxyuridine 5′-triphosphate nucleotidohydrolase, mitochondrial
	ATIC	P31939	Bifunctional purine biosynthesis protein PURH
	BCAT1	P54687	Branched-chain-amino-acid aminotransferase, cytosolic
	OAT	P04181	Ornithine aminotransferase, mitochondrial
	PKM	P14618	Pyruvate kinase
	LTA4H	P09960	Leukotriene A-4 hydrolase
	TPI1	P60174	Triosephosphate isomerase
ECM-receptor interaction ID: 04512	VWF	P04275	von Willebrand factor
	FN1	P02751	Fibronectin
	HSPG2	P98160	Heparin sulfate proteoglycan 2, basement membrane-specific heparan sulfate proteoglycan core protein
	COL5A1	P20908	Collagen α-1(V) chain
	THBS1	P07996	Thrombospondin-1
Focal adhesion ID: 04510	VWF	P04275	von Willebrand factor
	ACTB	P60709	Actin, cytoplasmic 1
	RAC2	P15153	Ras-related C3 botulinum toxin substrate 2
	FN1	P02751	Fibronectin
	COL5A1	P20908	Collagen α-1(V) chain
	THBS1	P07996	Thrombospondin-1
Glycolysis/Gluconeogenesis ID: 00010	ALDH2	P05091	Aldehyde dehydrogenase 2, mitochondrial
	PKM	P14618	Pyruvate kinase
	TPI1	P60174	Triosephosphate isomerase
Viral myocarditis ID: 05416	ACTB	P60709	Actin, cytoplasmic 1
	RAC2	P15153	Ras-related C3 botulinum toxin substrate 2
	ICAM1	P05362	Intracellular adhesion molecule 1

Open in a separate window

Figure 7

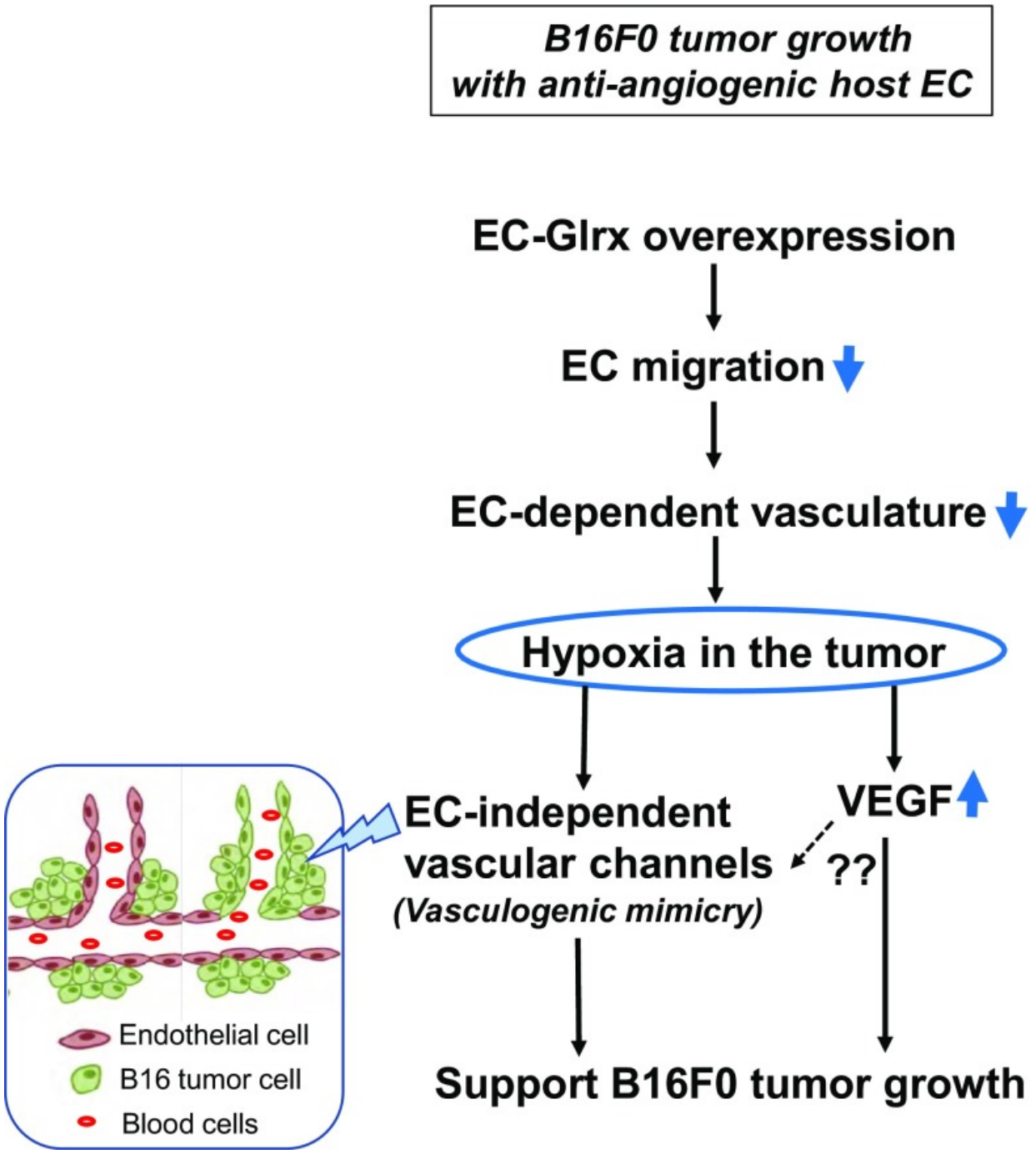

Open in a separate window

Hypothetical scheme for the mechanism of B16F0 growth in EC-Glrx TG mice.